Le Losq et al. Progress in Earth and Planetary Science (2015) 2:22
DOI 10.1186/s40645-015-0052-7

Progress in Earth and Planetary Science
a SpringerOpen Journal

RESEARCH ARTICLE Open Access

Water and magmas: insights about the water solution mechanisms in alkali silicate melts from infrared, Raman, and ^{29}Si solid-state NMR spectroscopies

Charles Le Losq*, Bjorn O. Mysen and George D. Cody

Abstract

Degassing of water during the ascent of hydrous magma in a volcanic edifice produces dramatic changes in the magma density and viscosity. This can profoundly affect the dynamics of volcanic eruptions. The water exsolution history, in turn, is driven by the water solubility and solution mechanisms in the silicate melt. Previous studies pointed to dissolved water in silicate glasses and melts existing as molecules (H_2O_{mol} species) and hydroxyl groups, OH. These latter OH groups commonly are considered bonded to Si^{4+} but may form other bonds, such as with alkali or alkaline-earth cations, for instance. Those forms of bonding influence the structure of hydrous melts in different ways and, therefore, their properties. As a result, exsolution of water from magmas may have different eruptive consequences depending on the initial bonding mechanisms of the dissolved water. However, despite their importance, the solution mechanisms of water in silicate melts are not clear. In particular, how chemical composition of melts affects water solubility and solution mechanism is not well understood. In the present experimental study, components of such information are reported via determination of how water interacts with the cationic network of alkali (Li, Na, and K) silicate quenched melts. Results from ^{29}Si single-pulse magic-angle spinning nuclear magnetic resonance (^{29}Si SP MAS NMR), infrared, and Raman spectroscopies show that decreasing the ionic radius of alkali metal cation in silicate melts results in decreasing fraction of water dissolved as OH groups. The nature of OH bonding also changes as the alkali ionic radius changes. Therefore, as the speciation and bonding of water controls the degree of polymerization of melts, water will have different effects on the transport properties of silicate melts depending on their chemical composition. This conclusion, in turn, may affect volcanic phenomena related to the viscous relaxation of hydrous magmas, such as for instance the fragmentation process that occurs during explosive eruptions.

Keywords: Melt; Glass; Structure; Water bonding; Water speciation; NMR spectroscopy; Raman spectroscopy; Viscosity; Magma; Fragmentation

Background

Water is typically the major volatile component in magmas and can reach concentrations up to ~6–7 wt. % in silicic magma chambers (e.g., see Blake 1984; Clemens 1984). When magmas migrate from their source up towards the Earth surface, water exsolution can result in large (up to several orders of magnitude) increases in magma viscosity because of the strong effect of water on the viscosity of silicate melts (Leonteva 1940; Saucier 1952; Friedman et al. 1963; Shaw 1963; Dingwell et al. 1996; Richet et al. 1996). Water exsolution is also accompanied by the formation of vapor bubbles that participate in decreasing the bulk density of the magma, reinforcing, in this way, the buoyant force that pushes the magma out of the Earth crust. In silica-poor magmas with viscosities lower than 10^6 Pa s at eruptive temperature, such as with basalts, gas bubbles can coalesce and escape from the magma (Thomas et al. 1994; Gardner et al. 1996). This situation usually results in gentle (lava flows) to slightly explosive

* Correspondence: clelosq@carnegiescience.edu
Geophysical Laboratory, Carnegie Institution of Washington, 5251 Broad Branch Road NW, Washington, DC 20015, USA

Springer

© 2015 Le Losq et al. **Open Access** This article is distributed under the terms of the Creative Commons Attribution 4.0 International License (http://creativecommons.org/licenses/by/4.0/), which permits unrestricted use, distribution, and reproduction in any medium, provided you give appropriate credit to the original author(s) and the source, provide a link to the Creative Commons license, and indicate if changes were made.

(lava fountain, strombolian explosion) eruptions. In contrast, for silica-rich compositions, the magma viscosity can be considerably higher than 10^6 Pa s at eruptive temperature, so that bubbles are trapped in the melts (Thomas et al. 1994; Gardner et al. 1996). Exsolution of water from such magmatic liquids often results in foaming. In such case, brittle fragmentation of the magmatic foam can occur, for example, when the elongation strain rate of the foam ascending in the conduit exceeds its viscous relaxation time (Papale 1999). This situation leads to explosive eruptions.

The effects of water on magma properties, together with their possible consequences as described above, result from how water affects the disordered tetrahedral silicate network of melts. A simple and commonly proposed solution mechanism of water in such melts involves the presence of H_2O molecules (H_2O_{mol}), which can react with the oxygens O of the silicate network to form OH groups:

$$H_2O_{mol(melt)} + O_{(melt)} <=> 2\ OH_{(melt)} \quad (1)$$

The solution mechanism illustrated in Eq. (1) is documented by numerous nuclear magnetic resonance (NMR) and infrared (IR) spectroscopic studies (e.g., Scholtze 1960; Moulson and Roberts 1961; Bartholomew et al. 1980; Stolper 1982; Kohn et al. 1989a, b; Zotov and Keppler 1998), which also indicated that OH groups seem bonded predominantly to Si (see also Farnan et al. 1987; Cody et al. 2005; Mysen and Cody 2005). Therefore, in this simple model, H_2O_{mol} reacts predominantly with bridging oxygens (BO), breaking T-O-T bonds (with T = Si, Al), so that Eq. (1) can be rewritten as:

$$H_2O_{mol(melt)} + T\text{–}O\text{–}T_{(melt)} <=> 2\ T\text{–}OH_{(melt)} \quad (2)$$

Equation (2) implies formation of non-bridging oxygens (NBO) when the reaction shifts to the right. However, reaction (2) does not always proceed to completion. Indeed, both H_2O_{mol} and OH groups coexist in silicate melts, and hence glasses, in proportions defined by temperature (Nowak and Behrens 1995; Sowerby and Keppler 1999; Behrens and Yamashita 2008) and apparently water concentration (e.g., Stolper 1982).

However, Eq. (2) is just one reaction describing the reaction of H_2O with the silicate network of silicate melts. Other dissolution mechanisms have been proposed, such as the formation of MOH bonds (with $M^{+,2+}$ a metallic ion) (Xue and Kanzaki 2004, 2006, 2008; Moretti et al. 2014) or the protonation of T-O-T bonds (H^+ does not break T-O-T bonds but is attached to it; see for example Kohn et al. 1989b, 1992, 1998 and references therein). Moreover, Eq. (2) does not consider the Q^n speciation often employed to describe the silicate structure (where n denotes the number of bridging oxygen in a silicate complex, see Schramm et al. 1984). For example, water can react with different Q^n species in sodium silicate melts depending on their initial water content and Na/Si ratio (Zotov and Keppler 1998; Mysen and Cody 2005; Mysen 2007). In addition, it appears likely that the electronic properties of the alkali and alkaline earth metal cations will affect the reaction mechanisms of water with the silicate network (Xue and Kanzaki 2004).

To understand, quantitatively, how water interacts with the silicate structure of glasses and melts, we examined the structure of alkali (Li^+, Na^+, K^+) tetrasilicate glasses using Raman and ^{29}Si SP MAS NMR spectroscopy. Existing infrared spectroscopic information (Le Losq et al. 2015a, b) was also used. By studying such compositionally simple systems, it is possible to isolate effects of individual components on the water solution behavior. Furthermore, the chosen glasses have anhydrous glass transition temperature, *Tg*, within a ~30 K range: the *Tg* of the sodium tetrasilicate glass is 751 K (Neuville 2006), that of the potassium tetrasilicate glass to 762 K (Neuville 1992), and that of the LS4 glass to 740 K (Voigt et al. 2005). They also have very similar distributions of silicate Q^n species (e.g., Maekawa et al. 1991). Those two characteristics (comparable anhydrous T_gs and Q^n distributions) allow us to emphasize differences that characterize the hydrous quenched melts rather than differences related to the starting anhydrous glasses.

Methods

Sample preparation

The starting materials as well as the hydrous glasses used for this study are the same as those reported in Le Losq et al. (2015a, b). We refer readers to these references for details on sample synthesis. The chemical compositions of glass starting materials are reported in Table 1.

Table 1 Chemical composition of LS4, NS4, and KS4 anhydrous glasses

		SiO_2	Li_2O	Na_2O	K_2O
LS4	nom. mol %	80.00	20.00	0.00	0.00
	nom. wt. %	88.94	11.08	0.00	0.00
	meas. wt. %	88.77 (94)	11.23 (75)	*n.a.*	*n.a.*
NS4	nom. mol %	80.0	0.00	20.00	0.00
	nom. wt. %	79.50	0.00	20.50	0.00
	meas. wt. %	80.38 (36)	*n.a.*	19.62 (31)	*n.a.*
KS4	nom. mol %	80.0	0.00	0.00	20.0
	nom. wt. %	71.84	0.00	0.00	28.16
	meas. wt. %	71.16 (49)	*n.a.*	*n.a.*	28.84 (28)

nom. mol %, nom. wt. %, and meas. wt. % refer respectively to the nominal compositions in mol and wt. % and to the measured composition in wt. %. Chemical compositions are from Le Losq et al. (2015a). Errors are given at the 1σ confidence interval

The ^{29}Si NMR signal from the anhydrous glasses suffers from a very long T_1 relaxation time. To reduce this T_1 relaxation time, a portion of the starting glasses was synthesized with a few hundred ppm Fe_2O_3, as previously done by Maekawa et al. (1991) to study similar alkali silicate glasses. To ensure homogeneous distribution of this small amount of iron oxide in the materials, the glass synthesis was done in two steps. The first step consisted in enriching a proportion of the starting glasses to 15 wt. % Fe_2O_3. During the second step, the iron-rich glasses were crushed and then mixed with crushed iron-free starting materials, in order to produce iron-enrichment in the 100–1000 ppm concentration range.

Quantitative analysis of the glasses by energy-dispersive x-ray spectrometry (EDS) was performed with a JEOL field-emission scanning electron microscope (FE-SEM) equipped with an Oxford silicon drift detector and using a 15 kV accelerating voltage and a 1.00 nA current. Measurements were performed scanning 25 by 25 micron areas. The EDS results were calibrated using the following standards: pyrope for O and Si, scapolite for Na, K1597 GI for K, and cossyrite for Fe. Calibration was based on a set of glass standards. The EDS results are within error of standards analyzed as unknowns.

The compositions of the Fe-doped glasses are essentially the same as those of the Fe-free starting materials. The iron contents are below detection limit (~200 ppm) for Fe-doped LS4, 1500 ± 300 ppm for Fe-doped NS4, and 700 ± 400 ppm for Fe-doped KS4 (mean values and errors from >10 individual measurements made at different spots). These Fe-doped glasses were used only to perform the ^{29}Si NMR measurements of anhydrous end-members. Optically, they are clear and colorless with the same Raman signal as iron-free starting glasses, indicating a homogeneous distribution of Fe in their structure. This is supported by SEM observations that show no clustering of iron at the micrometer scale. The ^{29}Si NMR data of the hydrous glasses were obtained on iron-free glasses. Indeed, in those water-bearing glasses, the ^{1}H nuclei that have a strong magnetic moment serve to aid the relaxation of ^{29}Si nuclei, as Fe at the ‰ level does in the anhydrous glasses.

Solid-state NMR spectroscopy

Silicon-29 solid-state NMR experiments were carried out with a Chemagnetics CMX Infinity 300 solid-state NMR spectrometer. The static field strength of the magnet is ~7.05 T, and the Larmor frequency of ^{29}Si is ~59 MHz at this magnetic field. ^{29}Si spectra were referenced to tetramethylsilane (TMS), defined as 0 ppm.

Single-pulse ^{29}Si MAS spectra of each glass were obtained by spinning the samples at 11 kHz. ^{29}Si excitation pulse widths corresponded to 30° tip angles. One thousand acquisitions separated by a 100 s recycling time were co-added. Proton decoupling was performed with continuous RF irradiation at 62.5 kHz. As indicated in the "Sample preparation" section, the anhydrous starting materials had a long ^{29}Si spin lattice T_1 relaxation time. For the KS4 glass, this long relaxation time resulted in a signal from ^{29}Si in Q^4 polymerized units much too low compared to a prediction of a mixture of 50 % Q^3:50 % Q^4 units based on glass chemical composition. Therefore, a portion of the anhydrous samples was doped with iron (see "Sample preparation" section) in order to decrease of the ^{29}Si T_1. The resulting signal from KS4 glass was much more intense than without the iron dopant and the spectra yielding Q^3–Q^4 proportion near the nominal 50:50. In hydrous glasses, which were iron-free, the protons played a similar role as iron, thus reducing the ^{29}Si spin–lattice relaxation time, so that spectra are directly quantitative. More details on the ^{29}Si single-pulse NMR experiments can be found in Cody et al. (2005).

Raman spectroscopy

Raman spectra were recorded with a Jasco NRS 3100 spectrometer, equipped with holographic gratings, a single monochromator, and a 1024 × 128 Andor DV401-F1 CCD Peltier-cooled detector operating at −70 °C. The 490 nm line of a coherent solid-state laser was used for sample excitation, with a power of ~44 mW on sample. The laser was focused on sample through a 50× Olympus lens. The groove density of the gratings was 2400 lines/mm, which results in an accuracy of ±3 cm^{-1}. Precision was ±1 cm^{-1}. Alignment of the Raman spectrometer was tested against the 520.7 cm^{-1} Raman peak of pure Si. All spectra reported in this study are unpolarized. The spectra were not corrected from temperature and excitation line effects (e.g., see Neuville et al. 2014, for further discussion about the relevance of such corrections) because thermal effects mostly affect the Raman intensity at frequency below 500 cm^{-1}, which does not contain much information relevant to the focus of the present study, and because excitation line effects are very small and in all cases will not affect our results since we used the same laser line for recording all spectra.

The Raman spectra were fitted using Gaussian peaks. A two-step fitting procedure was employed. As both the number of peaks and the frequency range of the fitted region are large, a first fitting step was carried out by using an equal peak width for all peaks. This fit was accomplished by using the *nlinfit* non-linear least-square optimization function of Matlab®. Then, in order to refine the models produced by *nlinfit*, the parameters and associated errors from those fits were injected in the pseudo-Newtonian algorithm described in Tarantola (2005) and used in Le Losq et al. (2014). This algorithm has the advantage of accounting of the a priori errors on the initial models (e.g., the errors on the estimations provided by the user or by *nlinfit* in

our case). Errors in peak areas were calculated by propagating the peak parameter errors.

Water concentration

Water concentrations [H_2O^{TOT}] of hydrous glasses were determined from IR absorption spectroscopy data of the NS4 compositions (for which molar absorption coefficients are available; Yamashita et al. 2008) and an FTIR-based calibration of the relative area of the OH fundamental stretch Raman band for the LS4 and KS4 glasses as described by Le Losq et al. (2015a). The resulting water contents together with glass synthesis conditions are reported in the Table 2.

The molar absorption coefficients of OH groups and H_2O_{mol} species for LS4 glasses have been estimated by using the IR data reported in Le Losq et al. (2015b) and the data treatment reported in Le Losq et al. (2015a), which follows the protocol described in Yamashita et al. (2008). A six-order polynomial baseline was fitted on spectra to derive a baseline under the 4500 and 5200 cm^{-1} IR absorption peaks (see Fig. 1, top left) and subtracted from spectra. Then, areas of the 4500 (A4500) and 5200 (A5200) cm^{-1} IR peaks, assigned to OH groups and H_2O_{mol} species respectively (Scholtze 1960; Moulson and Roberts 1961; Stolper 1982), have been measured (Table 2). The absorption coefficients of these two peaks (ε_{5200} and ε_{4500}, respectively) were calculated from the following relationship (Yamashita et al. 2008):

$$\frac{1820 \times \mathrm{A5200}}{d \times \rho \times \left[\mathrm{H_2O^{TOT}}\right]} = \varepsilon_{5200} - \frac{\varepsilon_{5200}}{\varepsilon_{4500}} \times \left[\frac{1820 \times \mathrm{A4500}}{d \times \rho \times \left[\mathrm{H_2O^{TOT}}\right]}\right] \quad (3)$$

with d, the thickness of the double-polished glass piece, and ρ, its density. The density of anhydrous LS4 glass was taken from Tischendorf et al. (1998). The density of hydrous glasses was then estimated by assuming a linear mixing between the molar volume of water and that of the glasses. In the water content range of the present study, such an assumption seems valid in light of the results of Yamashita et al. (2008) for sodium silicate glasses, and, on a larger dataset, with the results of Richet et al. (2000). According to results from those two studies, a partial molar volume of 12 cm^3 mol^{-1} for dissolved water was chosen. Such a value may overestimate slightly the actual molar volume of water in lithium silicate glasses, as inferred from results from ^1H NMR spectroscopy on these same glasses (Le Losq et al. 2015a). However, a change of the partial molar volume of water of 4 cm^3 mol^{-1} for instance can result in a maximum change of 4 L mol^{-1} cm^{-2} of the absorption coefficients. Such variations are incorporated in the reported error bars. By using Eq. (3), $\varepsilon_{5200} = 56 \pm 8$ (1σ) $L\ mol^{-1}\ cm^{-2}$ and $\varepsilon_{4500} = 70 \pm 7$ (1σ) L mol^{-1} cm^{-2} for the LS4 glass.

Use of the IR combination peaks at 4500 and 5200 cm^{-1} to determine water content of glasses is only possible when those peaks are well defined. In water-bearing alkali silicate glasses, an increase of the ionic radius of alkali (decreasing their ionic field strength) produces a decrease of the O-O distances around protons dissolved as H_2O_{mol} species and OH groups (Le Losq et al. 2015a). This perturbs significantly the frequency and intensity of the signal assigned to O-H stretching vibrations in IR and Raman spectra of hydrous alkali silicate glasses (Le Losq et al. 2015b). For example, in IR spectra of KS4 glasses, this signal extends to frequencies much lower than 3000 cm^{-1}, presenting several intensity maxima near ~2350, ~2800, and ~3600 cm^{-1}. This extended frequency range results in a poorly defined 4500 cm^{-1} combination band (Le Losq et al. 2015b) so that this

Table 2 Water concentration of glasses

Glass	nom. mol % H_2O	Conditions of synthesis	FTIR values					RAMAN
			A_{4200}	A_{5200}	[OH]	[H_2O_{mol}]	[H_2O^{TOT}]	[H_2O^{TOT}]
LS4	3.28	1650 °C	151 (12)	93 (9)	2.11 (35)	1.04 (22)	3.15 (41)	3.08 (60)
	9.40	1.5 GPa	325 (18)	452 (21)	4.56 (70)	5.06 (42)	9.61 (81)	10.09 (60)
	17.64		447 (21)	1109 (33)	6.26 (94)	12.42 (55)	18.68 (1.09)	18.74 (60)
NS4	3.28	1500 °C	155 (12)	3 (2)	3.85 (40)	0.07 (3)	3.92 (40)	3.44 (67)
	9.40	1.5 GPa	301 (17)	86 (9)	7.35 (63)	1.89 (20)	9.24 (66)	9.46 (67)
	17.64		403 (20)	440 (21)	9.52 (80)	9.35 (60)	18.87 (1.00)	17.54 (67)
KS4	3.28	1550 °C	-	-	3.98 (70)[a]	0.00 (0)[a]	-	3.98 (74)
	9.40	1.5 GPa	-	-	8.89 (70)[a]	0.73 (7)[a]	-	9.62 (74)
	17.64		-	-	13.65 (70)[a]	2.30 (24)[a]	-	15.95 (74)

Nom. refers to the nominal water concentrations. [H_2O_{mol}], [OH], and [H_2O^{TOT}] concentrations are in mol %. A_{4500} and A_{5200} are the integrated intensities of the IR peaks at ~4500 and ~5200 cm^{-1} that have been used to quantify the content of [OH] and [H_2O_{mol}] for the LS4 and NS4 glasses. FTIR and Raman values are from Le Losq et al. (2015a). Errors are given at the 1σ confidence interval

[a]Calculated with the calibration linking ^1H MAS NMR sideband area to H_2O_{mol} content shown in Fig. 1; the concentration of OH is estimated by difference to [H_2O_{mol}] measured with using Raman spectroscopy

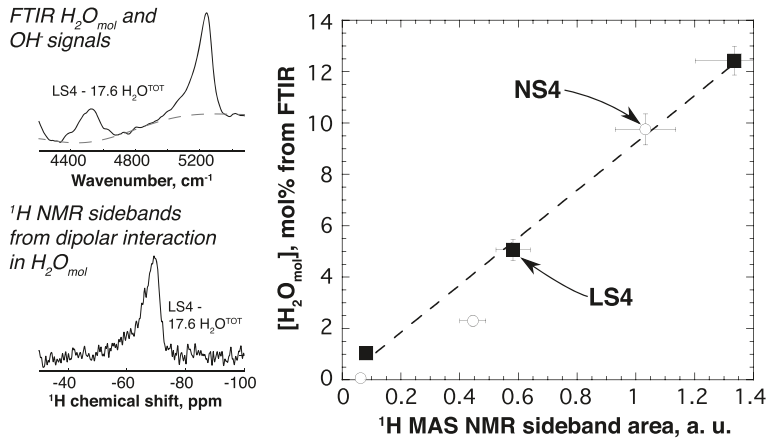

Fig. 1 Relationship between the area of ^1H MAS NMR sidebands, which arise from ^1H-^1H dipolar interaction in H_2O_{mol} species, and the concentration of the latters as measured by IR spectroscopy in the LS4 (plain squares) and NS4 (open circles) glasses. On the *left*, examples of the 4500 and 5200 cm^{-1} IR combination bands, assigned to OH and H_2O_{mol} species, respectively, and of one ^1H NMR sideband are shown for the LS4 glass containing 17.6 nom. mol% water. On the FTIR example, the *plain line* represents the experimental spectrum and the *dashed line* is a polynomial baseline defining the background (see text)

combination band cannot be used for measuring the concentration of OH groups. In such cases, an alternative to derive H_2O_{mol}/OH is to use the sidebands in ^1H MAS NMR spectra. These sidebands are residual signals from ^1H-^1H dipolar coupling, this interaction being strongly averaged by the fast magic angle spinning in the present experiments. The ^1H-^1H dipolar coupling is very strong in the case of H_2O_{mol} species and negligible in the case of isolated OH groups (Eckert et al. 1988). Therefore, in normalized ^1H NMR spectra acquired under similar conditions, sideband area would express the fraction of H_2O_{mol} species. Following this idea, Fig. 1 shows that the area of the sidebands ($A_{sidebands}$) of the ^1H MAS NMR spectra of LS4 and NS4 glasses, from Le7#146;Losq et al. (2015a), seem to be a linear function of the glasses H_2O_{mol} concentrations measured by IR. Particularly, the relationship seems nearly perfect for LS4 glasses. Slight deviations are observed for NS4 glasses. This can be rationalized with considering that most of the signal from O-H stretching vibrations is located above 3000 cm^{-1} in the IR spectra of LS4 glasses whereas it slightly extends toward lower frequency in the IR spectra of NS4 glasses (Le Losq et al. 2015b). This results in better defined ~ 4500 and ~ 5200 cm^{-1} combination bands in IR spectra of LS4 glasses than in those of NS4 glasses (Le Losq et al. 2015b), and hence, in higher accuracy on the calculated $[H_2O_{mol}]$ concentrations. Because of that, we can take the IR-based H_2O_{mol} concentrations and $A_{sidebands}$ from LS4 glasses as standards. Doing so, we obtain the relationship: mol % $H_2O_{mol} = 9.21 \pm 0.21 \times A_{sidebands}$. This equation allows us to determine the concentration of H_2O_{mol} species and of OH groups (by difference to the total water content) in the KS4 glasses (Table 2).

Results

Raman spectroscopy

The Raman-active vibrational modes of the silicate tetrahedral network give rise to numerous bands between 400 and 1400 cm^{-1} in the Raman spectra of silicate glasses (Fig. 2). A strong band near ~500 cm^{-1} is always observed. Smaller peaks and shoulders near 550 and 590–600 cm^{-1} are also present. Their intensity and frequency depend on glass composition. The respective intensity and frequencies of the contributions located between 450 and 650 cm^{-1} depend on the water content of the glasses and on the type of alkali metal (Fig. 2). Those signals arise from the bending/breathing modes of Si-O-Si bonds that link Q^n units (noted "Q^n-Q^n modes" in Fig. 2; see for instance Bell et al. 1968; Sen and Thorpe 1977; Furukawa et al. 1981 or McMillan 1984).

A band near 800 cm^{-1} is also observed in all of the Raman spectra (Fig. 2). For a given alkali, the intensity of this peak changes with water content, but not its shape. At given water content, increasing ionic radius of alkali results in decreasing the intensity of this peak. This band may arise from vibrations involving the motion of the Si in its oxygen cage (McMillan 1984), this being possibly related to the threefold—degenerate "rigid cage" vibrational mode of SiO_2 tetrahedra (Sen and Thorpe 1977; Galeener 1979). However, its origin is not firmly established.

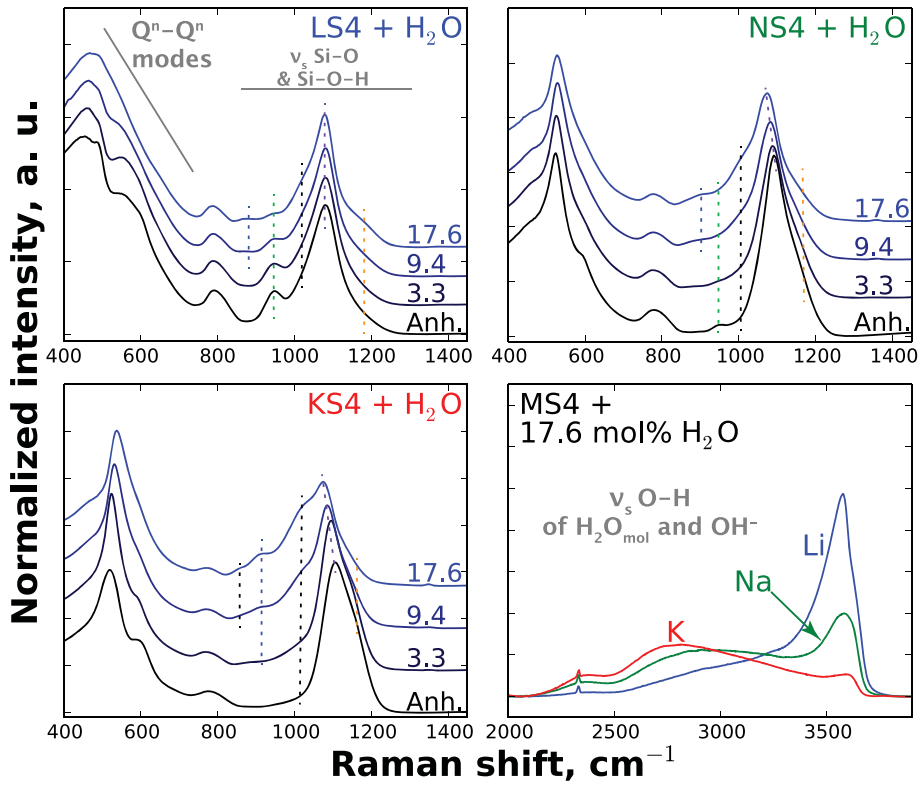

Fig. 2 Raman spectra of the lithium (LS4), sodium (NS4), and potassium (KS4) tetrasilicate glasses with 0.0 (Anh.), 3.3, 9.4, and 17.6 nom. mol % [H_2O^{TOT}]. Raman intensities are offset vertically for a better visibility, with the exception of the figure in *bottom right*. *Dashed lines* are used as visual markers of the signals contributing in the 820–1350 cm^{-1} portion of the spectra (see text). The small sharp peak located near 2330 cm^{-1} in the *lower right* figure is a signal from atmospheric N_2

Signals assigned to Si-O stretch vibrations in various Q^n units (ν_s Si-O in Fig. 2) form the broad envelope of bands between 850 and 1300 cm^{-1} (Brawer and White 1975, 1977; Virgo et al. 1980; Mysen et al. 1982; McMillan 1984; Neuville et al. 2014 and references therein). In hydrous alkali silicate glasses, a band often assigned to Si-O-H stretch vibrations contributes to the intensity in the 900–970 cm^{-1} frequency range (Stolen and Walrafen 1976; McMillan et al. 1993; Zotov and Keppler 1998; Malfait 2009). At frequencies higher than 1300 cm^{-1}, bands are observed between 2000 and 4000 cm^{-1} (Fig. 2, bottom right). These are assigned to O-H stretching (ν_s O-H) in H_2O_{mol} and OH groups (Scholtze 1960; Bartholomew et al. 1980; Wu 1980; Zotov and Keppler 1998). Their intensity and frequency depend on the chemical composition of the alkali silicate glasses. The larger the alkali ionic radius *r*, the lower the O-H stretch frequency (Fig. 2; see also Le Losq et al. 2015a; Le Losq et al. 2015b).

The topology of the 850–1300 cm^{-1} frequency region of the Raman spectra systematically varies as a function of both water content and ionic field strength of alkali in the glass (Fig. 2). This variation likely reflects changes of the Q^n species fractions. To quantify those changes, this portion of Raman spectra was fitted with Gaussian peaks. Such peak shape was used because it returns the best fitting results compared to other peak shapes (e.g., Lorentzian or Pseudo-Voigt shapes). This conclusion also is coherent with an expected pseudo Boltzmann distribution of Si-O vibrators in silicate melts in regards of their high thermal agitation and structural disorder at the glass transition temperature (Mysen et al. 1982). Table 3 summarizes the peaks used to perform the fits as well as their assignments and the references that substantiate those assignments.

The peak near 1100 cm^{-1} is assigned to Si-O stretching in Q^3 species. It is the most intense signal in the Raman spectra of all anhydrous glasses, whatever the alkali metal (Figs. 3 and 4). Areas of the peaks assigned to Si-O stretching in Q^2 and Q^4 species (near 950 and 1150–1200 cm^{-1}) respectively decrease and increase with increasing ionic radius of the alkali cation. These intensity variations indicate variations in the Q^n distribution as a function of the alkali ionic radius/field strength, similar

Table 3 Assignment of the peaks from curve-fitted Raman spectra

Raman shift, cm^{-1}	Attribution	Source
~850 cm^{-1}	ν_s Si-O in Q^1	Furukawa et al. (1981), Virgo et al. (1980), Mysen et al. (1982), McMillan (1984)
~880–910 cm^{-1}	ν_s Si-O-H	McMillan et al. (1993), Zotov and Keppler (1998), Malfait (2009), Spiekermann et al. (2012)
~960 cm^{-1}	ν_s Si-O in Q^2	Brawer and White (1975), Brawer and White (1977), Virgo et al. (1980), Furukawa et al. (1981), Mysen et al. (1982), McMillan (1984)
~1020 cm^{-1}	ν_s Si-BO in Q^n	Mysen et al. (1982), Spiekermann et al. (2012), Le Losq and Neuville (2013)
~1090 cm^{-1}	ν_s Si-O in Q^3	Brawer and White (1975), Virgo et al. (1980), Furukawa et al. (1981), Mysen et al. (1982)
~1140 cm^{-1}	ν_s Si-O in $Q^{4,II}$ ([a])	Mysen et al. (1982), Seifert et al. (1982), Mysen (1990), Neuville and Mysen (1996), Le Losq and Neuville (2013), Le Losq et al. (2014)
~1190 cm^{-1}	ν_s Si-O in $Q^{4,I}$ ([a])	Mysen et al. (1982), Seifert et al. (1982), Mysen (1990), Neuville and Mysen (1996), Le Losq and Neuville (2013), Le Losq et al. (2014)

[a]Two Gaussians named $Q^{4,II}$ and $Q^{4,I}$ are used for fitting the Si-O stretch of Q^4 because of its non-Gaussian shape. See Mysen et al. (1982), Seifert et al. (1982), Neuville and Mysen (1996), and Le Losq and Neuville (2013) for further discussion on this topic. In more depolymerized glasses, the signal of Q^4 becomes weak and only one band is needed (see in Fig. 2 the spectrum of KS4 + 17.6 mol % H_2O for instance)

to the conclusions drawn from previous ^{29}Si NMR (e.g., Maekawa et al. 1991) and Raman (e.g., Matson et al. 1983; Mysen 1990) spectra of binary alkali silicate glasses.

Solution of water in the melts quenched to glasses results in the appearance in the Raman spectra of a new peak near 900 cm^{-1} (Fig. 3). Its intensity increases with increasing water content, but the extent of this change depends on ionic radius of alkali (Fig. 3). The greater the alkali ionic radius, the larger the intensity of the ~900 cm^{-1} peak. Moreover, it appears that the type of alkali in the glass affects the frequency of this peak. For example, in the Raman spectra of glasses with 17.6 mol % H_2O, it shifts from 882 cm^{-1} for LS4 to 902 cm^{-1} for NS4 and 918 cm^{-1} for KS4. According to the study of Zotov and Keppler (1998) on sodium silicate glasses, this ~900 cm^{-1} peak may be assigned to Si-O-H stretching vibrations in Q^n species with Si-O-H bonds, regardless their number of bridging oxygens n. In pure hydrous silica, a peak near 976 cm^{-1} has been assigned to the signal of Si-O-H stretching vibrations (Stolen and Walrafen 1976). In hydrous aluminosilicate glasses, a peak located near 900 cm^{-1} has been assigned to a mixture of Si-O-H and Al-O-H vibrations, with the assumption that the Al-O-H stretching frequency is lower than that of Si-O-H (McMillan et al. 1993; Malfait 2009). However, recent results from molecular dynamic simulations (Spiekermann et al. 2012) questioned the attribution of the 976 cm^{-1} signal in pure hydrous silica and suggested that this peak may actually arise from the asymmetric Si-O stretching vibration of Q^2 units and that the Si-O-H stretching signal may form a shoulder near 920 cm^{-1} on the side of the 976 cm^{-1} peak. The fact that a peak near 900 cm^{-1} is detected and grows with solution of water in silicate glasses (Figs. 2 and 3, see also Zotov and Keppler 1998) may support such an interpretation, at least for silicate glasses.

The area of the ~950 cm^{-1} peak, assigned to Si-O stretching vibrations in Q^2, increases with solution of water in KS4 and NS4 glasses but decreases slightly in spectra of LS4 glasses (Fig. 4). The area of the ~1100 cm^{-1} peak, assigned to Si-O stretching vibrations in Q^3, seems to increase slightly with solution of water, but this effect is small (≤6 % with addition of 17.6 mol% H_2O, Fig. 4). Finally, the area of the two peaks at ~1150 and 1200 cm^{-1}, assigned to Si-O stretching vibrations in Q^4, varies differently as a function of water concentration and alkali ionic radius (Fig. 4). In Raman spectra of the NS4 and KS4 glasses, the area of these two peaks decreases with increasing water content (~10–20 % with addition of 17.6 mol % H_2O). In contrast, their area increases slightly (~3 %) with increasing water content from 0.0 up to 17.6 mol % in LS4 glasses.

There is another peak, near 850 cm^{-1}, in spectra of the KS4 glasses at high water concentration (Figs. 2 and 3). Its origin could be related to the presence of Q^1 species (e.g., see Mysen et al. 1982 or McMillan 1984), but Q^1 species are not detected by ^{29}Si NMR spectroscopy (see below and Fig. 5). This could be explained by an enhanced Raman signal of Q^1 species compared to other more polymerized Q^2, Q^3, or Q^4 species because of the increase of the Raman cross section of Q^n units that results from their depolymerization (decreasing n; see for instance Furukawa et al. 1981). Such effect has been observed for Q^2 species in sodium silicate glasses (Le Losq et al. 2014). Therefore, a very small proportion of Q^1 species (<1 %) may be present in the KS4 + 17.6 mol % H_2O and undetected by ^{29}Si NMR spectroscopy. This interpretation is speculative but does not affect the global observations because the 850 cm^{-1} signal intensity is negligible compared with those of the other signals.

^{29}Si single-pulse (SP) MAS NMR spectra

The ^{29}Si SP MAS NMR spectra of anhydrous glasses comprise two main peaks near −95 and −105 ppm

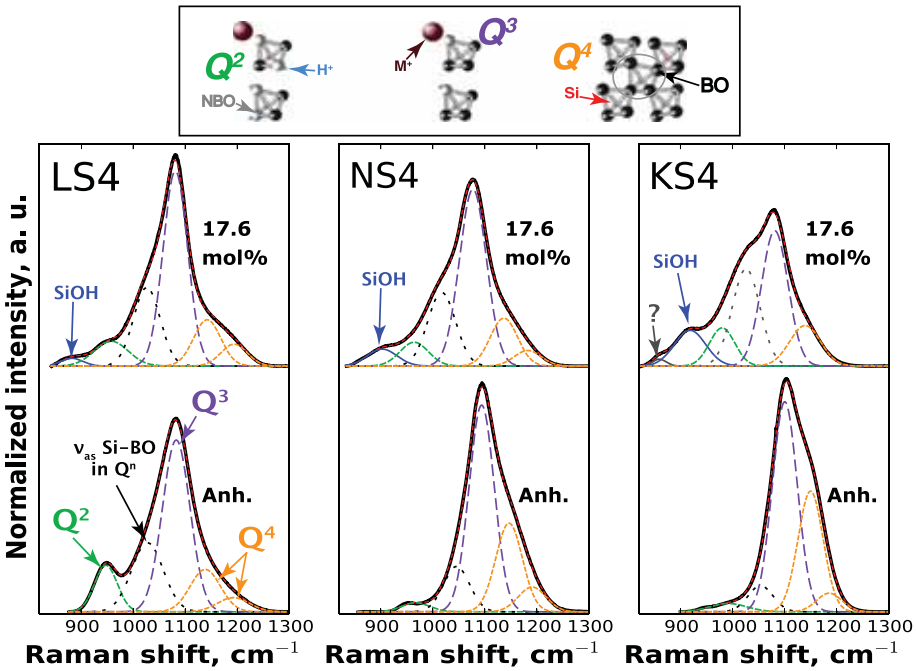

Fig. 3 Examples of curve-fitted Raman spectra of anhydrous and 17.6 mol% H_2O LS4 (*left*), NS4 (*middle*), and KS4 (*right*) glasses. Addition of water in the glasses clearly produces an increasing intensity near 900 cm^{-1}. It could be related to the stretching signal of Si-O-H bonds regardless of the Q^n specie carrying those bonds. Signal near 850 cm^{-1} in the Raman spectrum of KS4 + 17.6 mol % H_2O glass may be related to Q^1 species in the glass in negligible quantities. The various Q^n species are schematically represented at the top of the figure (ionic size is not at scale). *BO* bridging oxygen (Si-O-Si bonds), *NBO* non-bridging oxygen (Si-O-M or Si-O-H bonds, with M^+ an alkali)

(Fig. 5). A third contribution, located near −85 ppm, forms a shoulder in the spectrum of the anhydrous LS4 glass. The ~ −105, −95, and −85 ppm contributions are assigned to the signals of ^{29}Si in Q^4, Q^3, and Q^2 species, respectively (Lippmaa et al. 1980; Murdoch et al. 1985; Maekawa et al. 1991). The Q^3 and Q^4 contributions dominate the ^{29}Si SP MAS NMR spectra of anhydrous glasses (Fig. 5), in agreement with interpretation of Raman data (Figs. 3 and 4). The signal of Q^2 species is visible only in the spectrum of the LS4 anhydrous glass (Fig. 5). The relative intensities of Q^3 and $Q^4$$^{29}Si$ NMR signals vary slightly with ionic radius of alkali in anhydrous glasses. The global width of the ^{29}Si NMR signal also decreases with increasing ionic radius of alkali metal, and the frequency difference between Q^3 and Q^4 signals narrows (Fig. 5). The Q^4 frequency is the lowest in the spectrum of LS4 glass compared with those in the spectra of the NS4 and KS4 glasses. Such ^{29}Si NMR frequency changes can result from a modification of the shielding of the ^{29}Si nuclei with changing ionic radius of alkali. Maekawa et al. (1991) suggested that such shielding evolution may reflect changes in the third neighbor environments (e.g., Olivier et al. 2001), bond length, or bridging Si-O-Si angle as a function of ionic radius of alkali in silicate glasses.

In order to highlight the perturbations induced by the water addition in the glasses networks, the ^{29}Si SP MAS NMR spectra of the anhydrous glasses have been subtracted from those of hydrous glasses, giving residual ^{29}Si NMR spectra where positive and negative peaks can be observed (Fig. 5, bottom). Those peaks represent the changes of the proportions in the various Q^n species upon water addition. In all glasses, solution of water results in a reduction in intensity of the Q^4 peak, whereas that of the Q^3 peak increases (Fig. 5). However, the extent of this intensity change depends on ionic radius of alkali metal. The Q^3/Q^4 ratio changes only slightly for LS4 glass, whereas it increases strongly for KS4 glass. In the NMR spectra of NS4 and KS4 glasses, the intensity near −80/−85 ppm also increases upon water solution but not in spectra of LS4 glasses. It follows, therefore, that upon solution of water in the silicate glasses, Q^4 units are converted to Q^3 and Q^2 units, and that this effect gets more pronounced with increasing ionic radius of alkali.

Quantification of the effect of water on glass polymerization

The relative areas, A_{Q^n} $\left(\sum_{n=0}^{4} A_{Q^n} = 1\right)$, of the Raman peaks assigned to Si-O stretching in Q^n units (Fig. 4) can be related to the fraction of Q^n units through (Mysen 1990; Mysen and Frantz 1993):

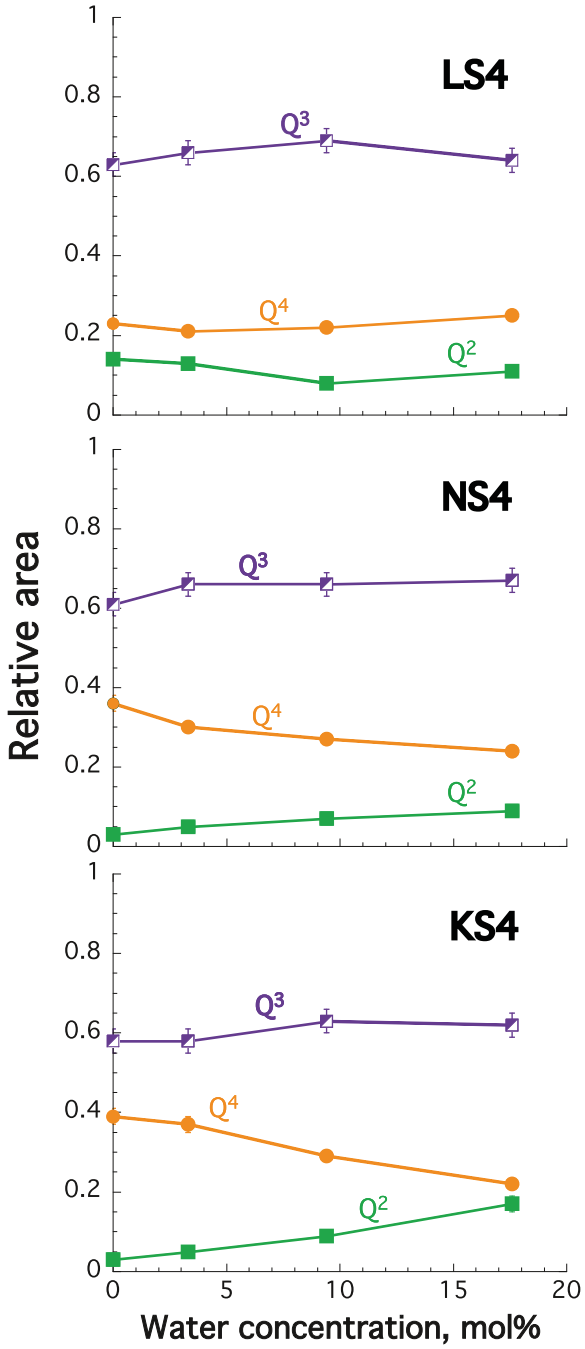

Fig. 4 Relative area of the Raman signals assigned to Q^2, Q^3, and Q^4 units composing the LS4 (*top*), NS4 (*middle*), and KS4 (*bottom*) glasses as a function of their nominal water concentration. Errors are given at the 1σ confidence interval. If not visible, they are smaller than the symbol sizes

$$[Q^n] = \theta^n A_{Q^n} \tag{4}$$

with θ^n a conversion factor that directly depends on the Raman cross section of the Si-O stretching vibrations in the Q^n units. The polymerization of a glass that contains a mixture of Q^2, Q^3 and Q^4units can be quantified by calculating the ratio of the mean number of NBOs other tetrahedral BOs as:

$$\mathrm{NBO/T} = 2[Q^2] + [Q^3] = 2 \times \theta^2 A_{Q^2} + \theta^3 A_{Q^3} \tag{5}$$

Between the anhydrous and hydrous glasses, we have the following equation:

$$\Delta\mathrm{NBO/T} = \mathrm{NBO/T^{hyd}} - \mathrm{NBO/T}^{anh} = 2[\Delta Q^2] + [\Delta Q^3], \tag{6}$$

where ΔQ^2 and ΔQ^3 are the variations of the Q^2 and Q^3 fractions between the anhydrous and hydrous glasses. The θ^2 and θ^3 values are near unity for sodium silicates and the effect of water solution on those values is negligible (Mysen 2007). Therefore, as a first approximation, we can neglect the θ^2 and θ^3 factors in Eqs. (5) and (6). It follows from the Raman data that addition of 17.6 mol % water in the LS4, NS4, and KS4 glasses results in $\Delta NBO/T$ of −0.04 ± 0.05, 0.18 ± 0.05, and 0.30 ± 0.05, respectively (Table 4).

Fitting ^{29}Si SP MAS NMR spectra with a set of Gaussian lines usually allows quantification of the Q^n fractions in silicate glasses (e.g., Maekawa et al. 1991). However, fitting the ^{29}Si SP MAS NMR spectra of the hydrous glasses is difficult because of the poor resolution of the shoulder associated to the signal of ^{29}Si in Q^2 units. Several solutions can be returned by the fitting procedure, and it is not clear how to discriminate between them. Fortunately, spectral fitting is not a requirement for quantifying the polymerization change induced by solution of water in glasses. Indeed, the areas of the peaks assigned to Q^2, Q^3, and Q^4 units in the residual ^{29}Si SP MAS NMR spectra (Fig. 5, bottom) are equivalent to the fractions of transformed Q^n units (ΔQ^n) upon solution of water. For the LS4 glasses, the ΔQ^3 signal area was measured between −87 and −102 ppm and the ΔQ^4 signal area between −102 and −122 ppm. In the spectra of the NS4 glasses, areas of the ΔQ^2, ΔQ^3, and ΔQ^4 signals were measured from −70 to −88, −88 to −101, and −101 to −120, respectively. For the spectra of KS4 glasses, the areas were measured from −70 to −91, −91 to −100, and −100 to −120, respectively. In order to evaluate the errors affecting the area determinations, the boundaries reported above were varied in a ±2–3 ppm uncertainty range. We have chosen such an uncertainty range because it is similar to the variations that affect the frequency of the peaks observed on the ^{29}Si MAS NMR spectra of the various glasses, and because it produces residual intensity variations higher than the noise level. As a result, such uncertainty range appears to be the best estimate for estimating the errors affecting the areas of residual signals.

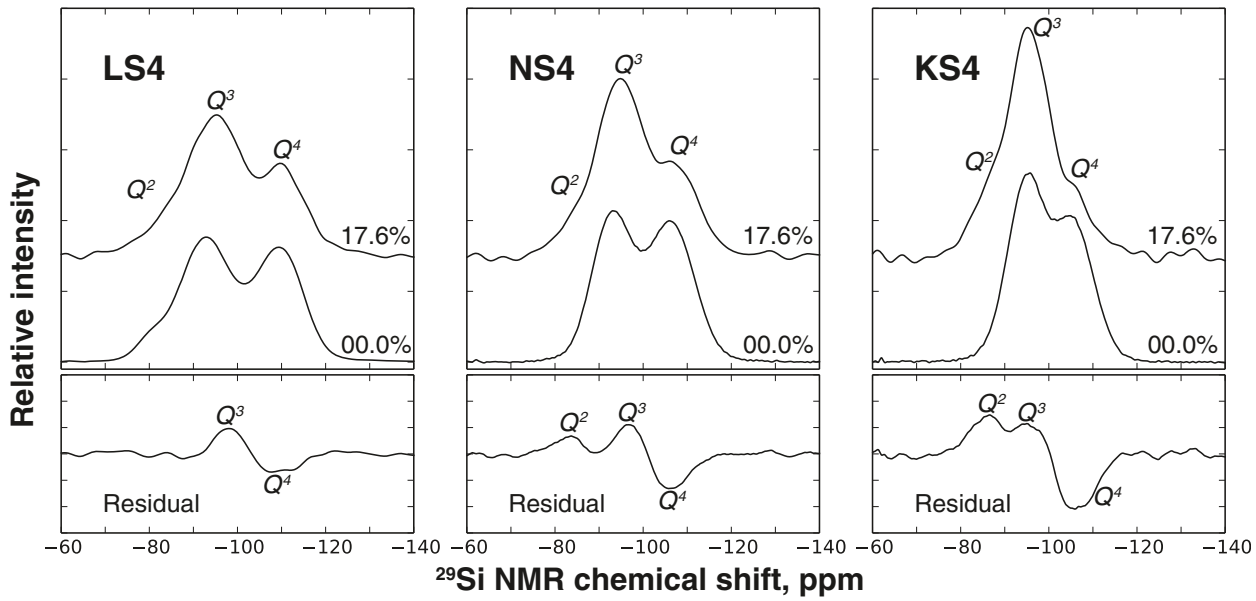

Fig. 5 *Top*: ^{29}Si single-pulse MAS (5 kHz) NMR spectra of the anhydrous and 17.6 nom. mol % H_2O LS4 (*left*), NS4 (*middle*), and KS4 (*right*) glasses. Intensities on spectra are normalized such that the total areas of the spectra are equal to unity. Changes in relative intensity and areas are thus directly proportional to the changes in the chemical concentrations of ^{29}Si in particular Q^n species. *Bottom*: residuals from the subtraction of the ^{29}Si NMR signals from hydrous glasses minus those from anhydrous glasses. Areas under the positive and negative peaks are quantitative and represent the fraction of transformed Q^n species upon hydration

The ΔQ^2 and ΔQ^3 values thus obtained can be used to compute $\Delta NBO/T$ with Eq. (6). The $\Delta NBO/T$ calculated from Raman data and from ^{29}Si SP MAS NMR difference spectra are in good agreement (Fig. 6 and Table 4) except for LS4 glass. Indeed, for the latter, the $\Delta NBO/T$ values obtained with the two different spectroscopic methods are different: -0.04 ± 0.05 (Raman) and 0.07 ± 0.01 (NMR). The Q^n speciation derived from the Raman spectra of LS4 glasses suggests almost no depolymerization of those glasses upon water solution. This conclusion differs somewhat from that drawn from the ^{29}Si NMR data, which indicate that there is a weak, but real, effect of water on the polymerization of LS4 glasses (Fig. 5). The errors affecting the fitting of Raman spectra might be too large to allow detection of the weak effect of water solution on the structure of LS4 glasses. Indeed, the Raman-derived $\Delta NBO/T$ values are affected by errors inherent to the fitting procedure (optimization error) as well as by errors inherent to the initial assumptions made for fitting (e.g., perfect Gaussian shape for the peaks). In this regards, NMR-derived $\Delta NBO/T$ values are more robust than the Raman-derived $\Delta NBO/T$ values because they do not rely on any fitting procedure but directly on calculations from raw data. This notwithstanding, both sets of values indicate a small effect of water addition on the degree of polymerization of the LS4 composition.

Table 4 ΔNBO/T, concentrations of total OH groups, SiOH, and *unknown* OH groups

	H_2O^{TOT} (Raman)	[OH]	ΔNBO/T (Raman)	[SiOH] (Raman)	[Unknown OH] (Raman)	ΔNBO/T (NMR)	[SiOH] (NMR)	[Unknown OH] (NMR)
LS4	3.08 (60)	2.11 (35)	0.02 (5)	0.63 (1.25)	1.47 (3.41)	-	-	-
	10.09 (60)	4.56 (70)	−0.05 (5)	0.00 (–)	4.56 (1.27)	-	-	-
	18.74 (60)	6.26 (94)	−0.04 (5)	0.00 (–)	6.26 (1.57)	0.07 (1)	2.77 (16)	3.49 (95)
NS4	3.44 (67)	3.85 (40)	0.08 (5)	3.24 (66)	0.61 (77)	-	-	-
	9.46 (67)	7.35 (63)	0.13 (5)	5.02 (43)	2.33 (76)	-	-	-
	17.54 (67)	9.52 (80)	0.18 (5)	7.28 (30)	2.24 (85)	0.18 (1)	7.17 (5)	2.35 (80)
KS4	3.98 (74)	3.98 (70)	0.04 (4)	1.42 (1.22)	2.56 (40)	-	-	-
	9.46 (74)	8.89 (70)	0.15 (5)	5.88 (32)	3.01 (77)	-	-	-
	15.95 (74)	13.65 (70)	0.30 (5)	12.08 (19)	1.57 (72)	0.34 (2)	13.63 (7)	0.02 (70)

Concentrations of OH, H_2O^{TOT}, SiOH, and *unknown* OH are in mol %

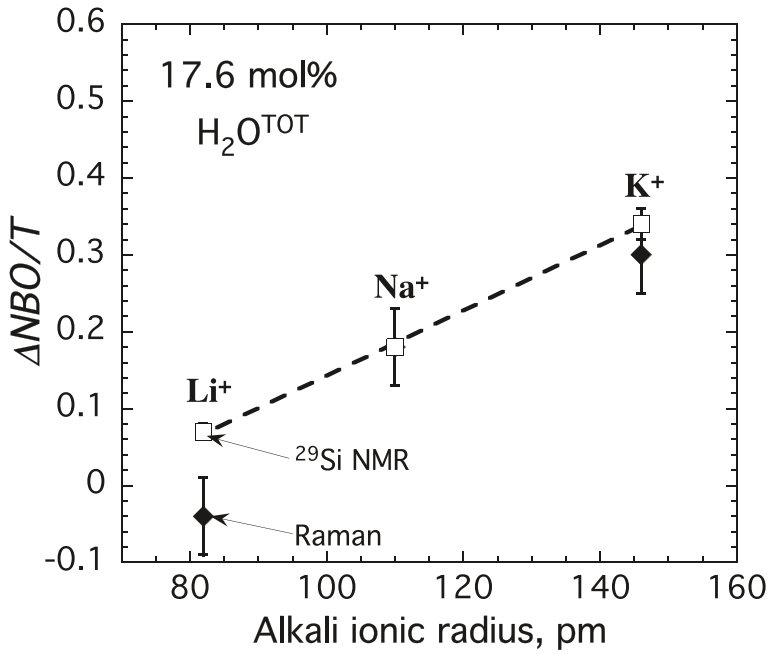

Fig. 6 Variation of the polymerization of the glasses (ΔNBO/T) upon addition of 17.6 nom. mol % water represented as a function of the ionic radius of alkali. ΔNBO/T (= $NBO/T_{anhydrous} - NBO/T_{17.6\ mol\%\ water}$) is calculated from the variations of the Q^n species as observed in Raman spectra (*plain symbols*) or in ^{29}Si NMR spectra (*open symbols*). Ionic radii of alkalis are from Whittaker and Muntus (1970), assuming sixfold oxygen-coordinated alkalis. The *black dotted line* is a linear fit of the ΔNBO/T vs ionic radius relationship for NMR data. For the Na-bearing silicate glass, Raman and ^{29}Si NMR give the same value, so that symbols are difficult to distinguish. *Error bars* are given at the 1σ confidence interval

Discussion

The dissolution of water into alkali silicate glasses results in their depolymerization, as shown by ^{29}Si NMR and Raman data (Figs. 4, 5, and 6). The Q^4 units transform to Q^3 and Q^2 units according to the reaction.

$$Q^4 \ <=> \ \phi Q^2 \ + (1-\phi)Q^3, \qquad (7)$$

where ϕ is a constant reflecting the partitioning of the NBOs (formed upon H_2O addition) between Q^3 and Q^2. The equilibrium constant K_7 of reaction 7 depends on ionic radius of alkali. The larger the radius, the greater the *ΔNBO/T* and, thus, the higher the K_7 (Fig. 6). This dependence likely is linked to the influence of ionic radius of alkali metal on the OH/H_2O_{mol} ratio. At given water content, the larger the ionic size of alkali cation, the higher this ratio (Fig. 7). The variations of ϕ seem primarily related to the extent of depolymerization of the silicate network because the ratio $\Delta Q^2/\Delta Q^3$ is correlated with *ΔNBO/T*. At low *ΔNBO/T*, and hence for *NBO/T* close to 0.5, ϕ is low and Q^3 units are produced by reaction (7). At high *ΔNBO/T*, and hence for *NBO/T* > 0.5, ϕ is high and Q^2 units formation may dominate.

The concentration of OH groups that form SiOH bonds upon hydration of the glasses can be determined by using the *ΔNBO/T* values derived from the Q^n-species abundances. This is possible because oxygen in the

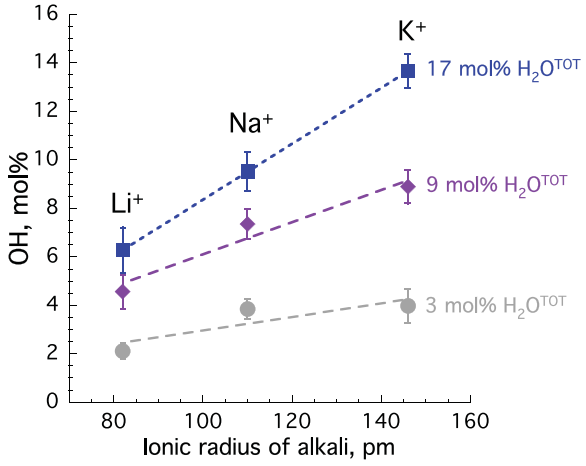

Fig. 7 Total OH group contents (mol %) of the alkali silicate glasses represented as a function of the alkali ionic radius (in picometers) for different water concentrations. Total OH group contents in KS4 glasses were determined by subtracting the H_2O_{mol} species contents determined with using ^{1}H MAS NMR spectra (see text and Fig. 1) to the total water content measured by Raman spectroscopy (see values in Table 2). The *dotted lines* are linear fits of the data. *Error bars* are given at the 1σ confidence interval

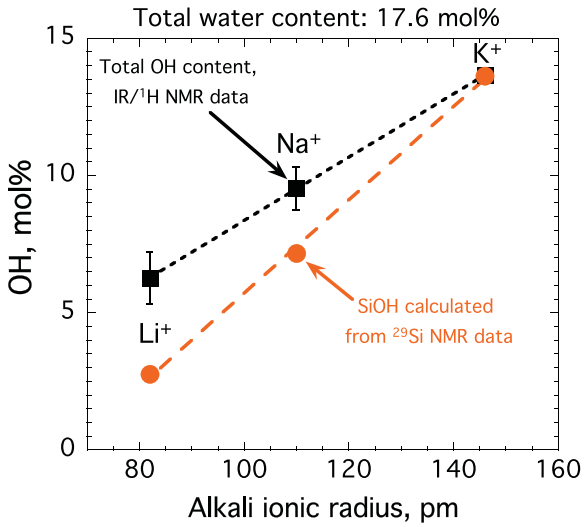

Fig. 8 Comparison between the concentration of OH groups measured with IR (LS4 and NS4 glasses) and ^{1}H NMR (KS4 glass) data and that of OH groups bonded to Si determined with using ^{29}Si NMR data for glasses with 17.6 mol % total H_2O. The *dotted lines* are linear fits of the data. *Error bars* are given at the 1σ confidence interval

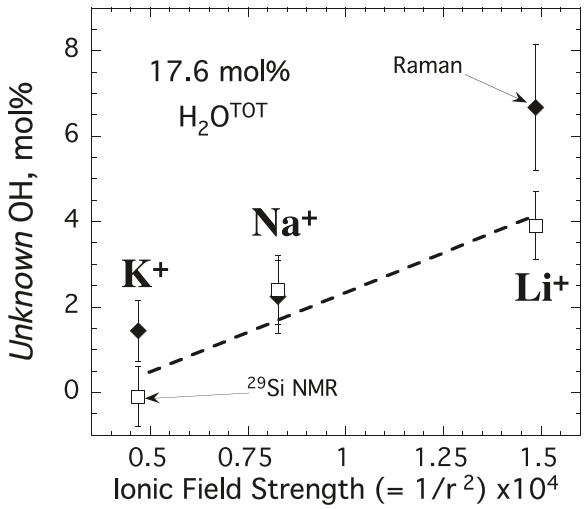

Fig. 9 Concentrations of *unknown* OH groups that do not participate in the depolymerization of the silicate network in the 17.6 mol % water glasses, represented as a function of the ionic field strength (IFS) of alkali. IFS = Z/r^2 with Z the electric charge and r the ionic radii of the alkalis (from Whittaker and Muntus 1970 assuming sixfold oxygen-coordinated alkalis). IFS was multiplied by 10^4 for clarity purpose. The *black dashed line* is a linear fit of the mol% unknown OH vs alkali IFS relationship calculated using NMR data. *Error bars* are given at the 1σ confidence interval

SiOH groups is non-bridging, so that SiOH group formation testifies to the depolymerization of the silicate network upon water solution (Eq. (2)). Figure 8 presents a comparison between the SiOH content determined with using *ΔNBO/T* derived from ^{29}Si SP MAS NMR data and the concentration of OH groups determined by using IR and ^{1}H MAS NMR data for glasses with 17.6 mol % water. At this water content, it appears that there are significant differences between these two sets of values for hydrous NS4 and LS4 glasses. For those glasses, the concentrations of SiOH groups are lower than those of OH groups detected by IR and ^{1}H MAS NMR spectroscopy. For the KS4 glass with 17.6 mol % water, the SiOH and the OH values obtained by the different methods agree. The SiOH fractions calculated from Raman-derived *ΔNBO/T* values confirm the above observations by showing a very similar trend following changes in ionic radius of alkali metal for glasses with 17.6 nom. mol % [H_2O^{TOT}] (Table 4).

The comparison in Fig. 8 and Table 4 between the SiOH concentrations retrieved through the ^{29}Si NMR data, validated by Raman results, and the total OH concentration from IR spectroscopy indicates that there is a significant fraction of OH groups in the NS4 and LS4 glasses that do not reflect depolymerization of the silicate network and for which we do not know the nature of their bonding. At 17.6 nom. mol % water, the concentration of those "unknown" OH groups increases with decreasing ionic radius, and hence, increasing ionic field strength of alkali metal (Fig. 9). It is negligible for the KS4 glass whereas it is maximum for the LS4 glass, which also has a negligible *ΔNBO/T*. It follows, therefore, that the chemical composition of the melt, in terms of ionic radius of the alkali metal, not only affects the speciation of water between OH groups and H_2O_{mol} species (Fig. 7), but also affects the bonding of the OH groups with the quenched melt structure (Figs. 8 and 9). The effect of the water concentration is less clear. From the Raman-derived SiOH contents, the fraction of *unknown* OH groups may increase in LS4 and NS4 with addition of water, whereas it may slightly decrease in the case of the KS4 glasses (Table 4). However, those values are difficult to interpret with confidence because they have not been validated by ^{29}Si NMR spectroscopy. This validation seems necessary in regards of the errors that can affect the *ΔNBO/T* determined from Raman spectroscopy, as shown by the data for LS4 (see Fig. 6).

Previous studies of hydrous sodium silicate glasses indicated that, at 80 mol% SiO_2, Eq. (2) appears to describe the mechanism of water solution in glasses (Zotov and Keppler 1998; Cody et al. 2005; Mysen and Cody 2005). The content of *unknown* OH is low in the NS4 glasses, near 2 mol % for a nominal total water content of 17.4 mol % (Table 4 and Fig. 9). The errors affecting the Q^n fractions determined by Raman or ^{29}Si NMR spectroscopy combined

with those affecting the determination of the concentrations of total OH groups render difficult the detection of such a low amount. This may explain why previous studies of sodium silicate glasses containing high silica contents did not see such small concentrations of OH groups not bonded to Si. However, in alkaline-earth and alkali silicate glasses with low silica contents (NBO/T > ~ 1), presence of OH groups not bonded to Si has been inferred (e.g., Xue and Kanzaki 2004; Cody et al. 2005; Mysen and Cody 2005).

Present data indicate that Eq. (2) alone cannot explain the solution mechanism of water in silicate glasses containing small alkali metals, such as Li and Na. Another mechanism implying a different bonding of OH group must be considered. The concentration of total OH groups measured by IR in LS4 glasses is much higher than that of OH bonded to Si (Figs. 8 and 9). This indicates that the *unknown* OH groups contribute to the 4100–4500 cm^{-1} portion of IR spectra, where the peak assigned to the combination of the OH groups vibrational modes is usually observed (e.g., see Fig. 1). To our knowledge, three hypotheses can explain observations: (1) the formation of MOH groups, where M is an alkali; (2) the protonation of bridging Si-O-Si bonds; or (3) the protonation of Si-O-M bonds.

Infrared spectra of crystalline alkali hydroxide show absorption bands in the 4000–4400 cm^{-1} portion of IR spectra. It has been proposed that they arise from the combination of the O-H fundamental stretching vibrations with the lattice modes (Buchanan 1959; Wickersheim 1959; Snyder et al. 1960). Therefore, contribution from MOH species in the 4100–4500 cm^{-1} range of the IR spectra of the present glasses seems possible, so that the observed *unknown* OH could be MOH species. In this line of thinking, we note that the IR peak near 4500–4600 cm^{-1} is also observed in hydrous soda-lime-borate glasses and assigned to the combination of the OH stretching with lattice vibrational modes (Bauer et al. 2015). Therefore, the 4500 cm^{-1} IR peak in hydrous glasses not only contains contributions of OH groups bonded to Si, as it has been previously inferred (e.g., Malfait 2009 and references therein), but also possible contributions from other OH species bonded to metallic elements or even boron, as shown by the data of Bauer et al. (2015).

Hypothesis (2) involves the protonation of Si-O-Si bonds and thus the formation of Si-(OH)-Si protonated bonds. A similar hypothesis has been proposed to account for water solution in glasses along the joined SiO_2-$NaAlO_2$ because of the apparently negligible changes of ^{29}Si and ^{27}Al NMR signals upon water addition to these glasses (Kohn et al. 1989b, 1992, 1998). Molecular orbital calculations indicate that both Si-OH and Si-(OH)-Si bonds give signals near 900 cm^{-1} (Kubicki and Sykes 2004), so that the OH groups involved in Si-(OH)-Si bonds will contribute to the IR combination peak near 4500 cm^{-1}. Therefore, the *unknown* OH groups may be involved in Si-(OH)-Si bonds.

Hypothesis (3) involves the protonation of Si-O-M bonds and the formation of Si-(OH)-M protonated bonds. In this hypothesis, it must be inferred that the Si-(OH)-M bonds give a signal similar to that of Si-(OH)-Si protonated bonds near 900 cm^{-1}, such that those bonds will contribute to the IR combination peak near 4500 cm^{-1}.

To discriminate between those hypotheses, several points have to be considered. First, the link between the size/ionic field strength (abbreviated IFS in the following) of the alkali and the concentration of *unknown* OH (Fig. 9) indicates that alkalis that form short (and thus strong) M-O bonds promote *unknown* OH groups. Considering hypothesis (3), it is unlikely that protonation of Si-O-M bonds occurs when the M-O bond strength is high, such as for Li-O bonds, because protonation of Si-O-M bonds may be more likely to occur for stabilizing Si-O-M bonds with low M-O bond strengths. Considering now hypothesis (2), protonation of Si-O-Si bonds would result in the appearance of positively charged $Si\text{-}(OH)^{+}$-Si bonds that would require charge balance by a negatively charged ion, i.e., by NBO oxygens or "free" oxygens O^{2-}. Such situation would require specific structural positions for the $Si\text{-}(OH)^{+}$-Si bonds and the compensating oxygens and thus seems unlikely to occur at high temperature in silicate melts that lack long- and medium-range orders. It should be noted that protonation of Si-O-Al bonds has been inferred in aluminosilicate compositions because it may help the electrical charge compensation of AlO_2 tetrahedral units, but it also has been strongly questioned (see introduction of Malfait and Xue 2010 and references cited therein). Indeed, the most recent data point to formation of SiOH and AlOH groups in aluminosilicate glasses and not to protonation of bridging oxygen (e.g., see Xue and Kanzaki 2009, Malfait and Xue 2010 and references cited therein).

Therefore, the most plausible hypothesis to explain the observations of a fraction of OH groups not bonded to Si in the alkali silicate glasses is the formation of MOH groups. In particular, this hypothesis explains the link between the alkali IFS and the concentration of *unknown* OH groups (Fig. 9): metal cations with strong M-O bonds may help stabilizing MOH complexes, in agreement with interpretations of Xue and Kanzaki (2004). In addition, this hypothesis is supported by ^{1}H MAS and ^{1}H->^{29}Si->^{1}H CP MAS NMR data on Ca and Mg silicate glasses that indicate the present of MOH groups in such compositions (Xue 2009). Therefore, from the above discussion, the *unknown* OH groups likely are bonded to alkali elements, forming MOH molecular complexes.

We propose the following framework to explain the spectroscopic observations. A condition for the reaction of H_2O_{mol} species with the network of silicate melts is the self-ionization of H_2O_{mol} species (Moretti et al. 2014):

$$H_2O_{mol\,(melt)} <=> H^+{}_{(melt)} + OH^-{}_{(melt)} \quad (8)$$

When H_2O_{mol} reacts with Si-O-Si bonds, H^+ and OH^- are consumed to form SiOH bonds, leading to the process described by Eq. (2). In the present silica-rich glasses, H^+ and OH preferentially react with Q^4 bonds to form Q^2 and Q^3 species (Fig. 5), so that the depolymerization mechanism can be described by Eq. (7), confirming previous observations in similar composition (Zotov and Keppler 1998; Cody et al. 2005; Xue and Kanzaki 2004; Mysen and Cody 2005). Decreasing the ionic radius, and hence, increasing the IFS of alkali metal in silicate melts inhibits the self-ionization reaction of water (Fig. 7) but also promotes reaction of H^+ and OH^- with the non-bridging oxygen NBO and the alkalis of the Si-O-M bonds (Fig. 9) following:

$$H_2O_{mol} + SiOM <=> SiOH + MOH \quad (9)$$

Such a mechanism was proposed by Xue and Kanzaki (2004), who suggested the formation of MOH complexes in highly depolymerized Ca, Mg, and Na silicate melts (NBO/T > 1) on the basis of molecular dynamic calculations and ^{1}H MAS NMR observations. They also proposed the following reaction (see also Mysen and Cody 2005):

$$2\ SiOM + H_2O_{mol} <=> SiOSi + 2\ MOH, \quad (10)$$

Formation of MOH species can result in no change (Eq. (9)) or even in an increase (Eq. (10)) of the melt polymerization. Xue and Kanzaki (2004) indicated that such mechanisms mostly concerned depolymerized melts (NBO/T > ~1) (see also the discussion in Xue and Kanzaki 2009), in agreement with the findings of Cody et al. (2005) and Mysen and Cody (2005). However, the water solution mechanism for the LS4 glass is best described by the combination of Eqs. (8) and (9). Therefore, the present data support the solution mechanism described with Eq. (9) in melts with relatively high silica contents (NBO/T ~ 0.5) that contain network modifier elements with high IFS (Fig. 9).

According to the present data (Figs. 7, 8, and 9), IFS of network modifying alkali metals plays an important role in defining the equilibrium constants of Eqs. (8) (self-ionization of water), (2) (SiOH formation), (9) and (10) (MOH formation). The origin of such role could arise from electronic/steric considerations, hydration shell formation, or volume effects around alkalis governed by their size/IFS (Le Losq et al. 2015a). For instance, electronic effects may influence the hydrolysis energy of Si-O-Si and Si-O-M bonds, and hence, the equilibrium constants of reactions (2), (9), and (10) (i.e., see discussion in Xue and Kanzaki 2004). Volume effects cannot be excluded. For instance, large alkalis may inhibit the presence of cavities in which H_2O_{mol} species might be contained, and hence, will result in a large equilibrium constant for reaction (8). Formation of hydration shell around small alkalis may also help explaining the speciation of water (Fig. 7). Finally, IFS of metal cations may also affect the stability of MOH molecular complexes (Xue and Kanzaki 2004), explaining the link between the IFS of metal cations and the concentration of observed MOH groups (Fig. 9). However, the present data do not allow us to discriminate between those hypotheses. In addition, it cannot be excluded that several mechanisms play roles at the same time. Despite that, it is clear that the influence of the alkali IFS on the speciation, environment, and bonding of water in silicate quenched melts results in differences in water solubility (Mysen and Acton 1999; Mysen and Cody 2004) and partial molar volume (Mysen and Cody 2004). Beyond such concerns, the differences of bonding and speciation of water in hydrous glasses as a function of their chemical composition probably also result in variations in their physical properties such as their glass transition temperature and density.

Conclusions

The water speciation in glasses is that of the melts at their glass transition temperature, *Tg* (see for instance Nowak and Behrens 1995). Present results show that IFS of alkali affects the speciation of dissolved water between H_2O_{mol} species and OH groups, as well as the OH bonding mechanisms in glasses, and hence, in melts at their *Tg*. Therefore, the chemical composition of silicate melts affects the solution mechanisms of water (Figs. 7, 8, and 9), resulting in different effects on melt structures at *Tg* (Figs. 3, 4, 5, and 6). In addition, variations in the solubility of water with ionic radius of the alkali in tetrasilicate melts (see data for NS4 and KS4 in Mysen and Cody 2004) at given temperature and pressure indicate that such interplay between the melt composition, water solution mechanism, and the melt structure affects the solubility of water. As a result, such interplay probably drives the water exsolution history of magmas.

In addition to such effect, this complex interplay implies that water will affect differently the rheological properties of magmas depending on their composition. Indeed, the strong changes in melt structure (Figs. 4, 5, and 6) that accompanies variations in water solution mechanism (Figs. 7, 8, and 9) probably result in different glass transition temperatures for the hydrous alkali tetrasilicate

glasses at given [H_2O^{TOT}], and, as a corollary, in different viscosity vs temperature paths. The present data do not allow us to make inferences on the extent of those differences, but they are expected to occur in view of the intimate link between the structure and the viscosity of alkali silicate melts (e.g., see Mysen and Richet 2005 for further details). Therefore, magmas with different chemical compositions will not only present different degassing paths, but also they will present different changes in their viscosity as a function of water content and temperature. Such consideration might be important for assessing about volcanic processes intimately linked to the viscous relaxation of magmas, such as the fragmentation that occurs in explosive eruptions (Papale 1999). Indeed, following the above ideas, the complex interplay between the magma composition, molecular structure, viscous properties, and the water solution mechanisms and solubility may influence the fragmentation threshold of magmas.

Abbreviations

EDS: energy-dispersive x-ray spectroscopy; SP: single pulse; MAS: magic angle spinning; NMR: nuclear magnetic resonance; IR: infrared; IFS: ionic field strength.

Competing interests

The authors declare that they have no competing interests.

Authors' contributions

BOM and GDC proposed the study. CLL made the experimental study, treated and interpreted data, and drafted the manuscript. BOM helped CLL for the experiments and lead the study. GDC performed the NMR experiments with the help of CLL. BOM and GDC collaborated with CLL in the construction of the manuscript. All authors read and approve the final manuscript.

Authors' information

CLL performed this study as a Postdoctoral Fellow at the Geophysical Laboratory, Carnegie Institution of Science, Washington DC, USA, under the mentorship of BOM and GDC, respectively Senior Scientist at, and Acting Director of the Geophysical Laboratory.

Acknowledgements

This research was partially supported by grants EAR1212754 and EAR1250449 to BOM and the NASA Astrobiology Institute. All NMR experiments were performed at the W. M. Keck Solid State NMR Facility at the Geophysical Laboratory, supported in part by the W. M. Keck Foundation, the NSF, and the Carnegie Institution of Washington.
This paper belongs to the Solid Earth Sciences section.

Received: 19 February 2015 Accepted: 2 August 2015
Published online: 14 August 2015

References

Bartholomew RF, Butler BL, Hoover HL, Wu CK (1980) Infrared spectra of a water-containing glass. J Am Ceram Soc 63:481–485
Bauer U, Behrens H, Fechtelkord M, Reinsch S, Deubener J (2015) Water- and boron speciation in hydrous soda-lime-borate glasses. J Non Cryst Solids 423–424:58–67
Behrens H, Yamashita S (2008) Water speciation in hydrous sodium tetrasilicate and hexasilicate melts: constraint from high temperature NIR spectroscopy. Chem Geol 256:306–315
Bell RJ, Bird NF, Dean P (1968) The vibrational spectra of vitreous silica, germania and beryllium fluoride. J Physics C (Proc phys soc) 1:299–303
Blake S (1984) Volatile oversaturation during the evolution of silicic magma chambers as an eruption trigger. J Geophys Res 89:8237–8244
Brawer SA, White WB (1975) Raman spectroscopic investigation of the structure of silicate glasses. I. The binary alkali silicates*. J Chem Phys 63:2421–2432
Brawer SA, White WB (1977) Raman spectroscopic investigation of the structure of silicate glasses (II). Soda-alkaline earth-alumina ternary and quaternary glasses. J Non Cryst Solids 23:261–278
Buchanan RA (1959) Near infrared spectra of crystalline alkali hydroxides. J Chem Phys 31:870–874
Clemens JD (1984) Water contents of silicic to intermediate magmas. Lithos 17:273–28
Cody GD, Mysen BO, Lee SK (2005) Structure vs. composition: a solid-state ^{1}H and ^{29}Si NMR study of quenched glasses along the Na_2O-SiO_2-H_2O join. Geochim Cosmochim Acta 69:2373–2384
Dingwell DB, Romano C, Hess KU (1996) The effect of water on the viscosity of a haplogranitic melt under P-T-X conditions relevant to silicic volcanism. Contribut Mineral Petrol 124:19–28
Eckert H, Yesinowski JP, Silver LA, Stolper EM (1988) Water in silicate glasses: quantification and structural studies by ^{1}H solid echo and MAS-NMR methods. J Phys Chem 92:2055–2064
Farnan I, Kohn SC, Dupree R (1987) A study of the structural role of water in hydrous silica glass using cross-polarisation magic angle spinning NMR. Geochim Cosmochim Acta 51:2869–2873
Friedman I, Long W, Smith RL (1963) Viscosity and water content of rhyolite glass. J Geophys Res 68:6524–6535
Furukawa T, Fox KE, White WB (1981) Raman spectroscopic investigation of the structure of silicate glasses. III. Raman intensities and structural units in sodium silicate glasses. J Chem Phys 75:3226–3237
Galeener FL (1979) Band limits and the vibrational spectra of tetrahedral glasses. Phys Rev B 19:4292–4397
Gardner JE, Thomas RME, Jaupart C, Tait S (1996) Fragmentation of magma during Plinian volcanic eruptions. Bull Volcanol 58:144–162
Kohn SC, Dupree R, Mortuza MG (1992) The interaction between water and aluminosilicate magmas. Chem Geol 96:399–409
Kohn SC, Dupree R, Smith ME (1989a) Proton environments and hydrogen-bonding in hydrous silicate glasses from proton NMR. Nature 337:539–541
Kohn SC, Dupree R, Smith ME (1989b) A multinuclear magnetic resonance study of the structure of hydrous albite glass. Geochim Cosmochim Acta 53:2925–2935
Kohn SC, Smith ME, Dirken PJ, Van Eck ERH, Kentgens APM, Dupree R (1998) Sodium environment in dry and hydrous albite glasses: Improved ^{23}Na solid state NMR data and their implications for water dissolution mechanisms. Geochim Cosmochim Acta 62:79–87
Kubicki JD, Sykes DG (2004) Ab initio calculation of ^{1}H, ^{17}O, ^{27}Al and ^{29}Si NMR parameters, vibrational frequencies and bonding energetics in hydrous silicate and Na-aluminosilicate glasses. Geochim Cosmochim Acta 68:3909–3918
Le Losq C, Neuville DR (2013) Effect of the Na/K mixing on the structure and the rheology of tectosilicate silica-rich melts. Chem Geol 346:57–71
Le Losq C, Cody GD, Mysen BO (2015a) Alkali influence on the water speciation and the environment of protons in silicate glasses revealed by ^{1}H MAS NMR spectroscopy. Am Mineral 100:466–473
Le Losq C, Cody GD, Mysen BO (2015b) Complex stretching signal of OH groups in silicate glasses: implication for the use of the 4500 cm^{-1} IR peak as a marker of OH^{-} groups concentration. Am Mineral 100:945–950
Le Losq C, Neuville DR, Florian P, Henderson GS, Massiot D (2014) The role of Al^{3+} on rheology and structural changes of sodium silicate and aluminosilicate glasses and melts. Geochim Cosmochim Acta 126:495–517
Leonteva A (1940) Measurements of the viscosity of obsidian and of hydrated glasses. *Izvestiya Akademii Nauk SSSR*. Ser Geol 2:44–54
Lippmaa E, Mägi M, Samoson A, Engelhardt G, Grimmer A-R (1980) Structural studies of silicates by solid-state high-resolution ^{29}Si NMR. J Am Chem Soc 102:4889–4893
Maekawa H, Maekawa T, Kawamura K, Yokohama T (1991) The structural groups of alkali silicate glasses determined from ^{29}Si MAS-NMR. J Non Cryst Solids 127:53–64
Malfait WJ (2009) The 4500 cm–1 infrared absorption band in hydrous aluminosilicate glasses is a combination band of the fundamental {Si, Al}-OH and O-H vibrations. Am Mineral 94:849–852
Malfait WJ, Xue X (2010) The nature of hydroxyl groups in aluminosilicate glasses: Quantifying Si-OH and Al-OH abundances along the SiO_2-$NaAlSiO_4$ join by ^{1}H, ^{27}Al-^{1}H and ^{29}Si-^{1}H NMR spectroscopy. Geochim Cosmochim Acta 74:719–737
Matson DW, Sharma SK, Philpotts JA (1983) The structure of high-silica alkali-silicate glasses. A Raman spectroscopic investigation. J Non Cryst Solids 58:323–352
McMillan PF (1984) Structural studies of silicate glasses and melts—applications and limitations of Raman spectroscopy. Am Mineral 69:622–644

McMillan PF, Poe BT, Stanton TR, Remmele RL (1993) A Raman spectroscopic study of H/D isotopically substituted hydrous aluminosilicate glasses. Phys Chem Min 19:454–459
Moretti R, Le Losq C, Neuville DR (2014) The amphoteric behavior of water in silicate melts from the point of view of their ionic-polymeric constitution. Chem Geol 367:23–33
Moulson AJ, Roberts JP (1961) Water in silica glass. Trans Faraday Soc 57:1208–1216
Murdoch JB, Stebbins JF, Carmichael ISE (1985) High-resolution ^{29}Si NMR study of silicate and aluminosilicate glasses: the effect of network-modifying cations. Am Mineral 70:332–343
Mysen BO (1990) Role of Al in depolymerized, peralkaline aluminosilicate melts in the systems Li_2O-Al_2O_3-SiO_2, Na_2O-Al_2O_3-SiO_2, and K_2O-Al_2O_3-SiO_2. Am Mineral 75:120–134
Mysen BO (2007) The solution behavior of H_2O in peralkaline aluminosilicate melts at high pressure with implications for properties of hydrous melts. Geochim Cosmochim Acta 71:1820–1834
Mysen BO, Acton M (1999) Water in H_2O-saturated magma-fluid systems: solubility behavior in K_2O-Al_2O_3-SiO_2-H_2O to 2.0 GPa and 1300 °C. Geochim Cosmochim Acta 63:3799–3815
Mysen BO, Cody G (2005) Solution mechanisms of H_2O in depolymerized peralkaline melts. Geochim Cosmochim Acta 69:5557–5566
Mysen BO, Cody G (2004) Solubility and solution mechanism of H_2O in alkali silicate melts and glasses at high pressure and temperature. Geochim Cosmochim Acta 68:5113–5126
Mysen BO, Frantz JD (1993) Structure and properties of alkali silicate melts at magmatic temperatures. Eur J Mineral 5:393–407
Mysen BO, Richet P (2005) Silicate glasses and melts—properties and structure. Developments in Geochemistry 10. Elsevier B.V, Amsterdam
Mysen BO, Finger LW, Virgo D, Seifert FA (1982) Curve-fitting of Raman spectra of silicate glasses. Am Mineral 67:686–695
Neuville, D. R. (1992) Etude des propriétés thermodynamiques et rheologiques des silicates fondus. Ph.D. Thesis of the Université Paris 7, 274.
Neuville DR (2006) Viscosity, structure and mixing in (Ca, Na) silicate melts. Chem Geol 229:28–41
Neuville DR, Mysen BO (1996) Role of aluminium in the silicate network: in situ, high-temperature study of glasses and melts on the join SiO_2-$NaAlO_2$. Geochim Cosmochim Acta 60:1727–1737
Neuville DR, de Ligny D, Henderson GS (2014) Advances in Raman spectroscopy applied to Earth and Material Sciences. Rev Mineral Geochem 78:509–541
Nowak M, Behrens H (1995) The speciation of water in haplogranitic glasses and melts determined by in situ near-infrared spectroscopy. Geochim Cosmochim Acta 59:3445–3450
Olivier L, Yuan X, Cormack AN, Jäger C (2001) Combined ^{29}Si double quantum NMR and MD simulation studies of network connectivities of binary $Na_2O.SiO_2$ glasses: new prospects and problems. J Non Cryst Solids 293–295:53–66
Papale P (1999) Strain-induced magma fragmentation in explosive eruptions. Nature 397:425–428
Richet P, Lejeune A-M, Holtz F, Roux J (1996) Water and the viscosity of andesite melts. Chem Geol 128:185–197
Richet P, Whittington AG, Holtz F, Behrens H, Ohlhorst S, Wilke M (2000) Water and the density of silicate glasses. Contribut Mineral Petrol 138:337–347
Saucier H (1952) Quelques expériences sur la viscosité à haute température de verres ayant la composition d'un granite. Influence de la vapeur d'eau sous pression. Bull de la Société Française de Minéralogie et de Cristallographie 75:1–45
Scholtze H (1960) Zur Frage der unterscheidung zwischen H_2O-Molekeln und OH-gruppen in gläsern und mineralen. Naturwissenschaften 47:226–227
Schramm CM, de Jong BHWS, Parziale VE (1984) ^{29}Si magic angle spinning NMR study on local silicon environments in amorphous and crystalline lithium silicates. J Am Chem Soc 106:4396–4402
Seifert F, Mysen BO, Virgo D (1982) Three-dimensional network structure of quenched melts (glass) in the systems SiO_2-$NaAlO_2$, SiO_2-$CaAl_2O_4$ and SiO_2-$MgAl_2O_4$. Am Mineral 67:696–717
Sen PN, Thorpe MF (1977) Phonons in AX_2 glasses: from molecular to band-like modes. Phys Rev B 15:4030–4038
Shaw HR (1963) Obsidian-H_2O viscosities at 1000 and 2000 bars in the temperature range 700° to 900 °C. J Geophys Res 68:6337–6343
Snyder RG, Kumamoto J, Ibers JA (1960) Vibrational spectrum of crystalline potassium hydroxide. J Chem Phys 33:1171–1177
Sowerby JR, Keppler H (1999) Water speciation in rhyolitic melt determined by in-situ infrared spectroscopy. Am Mineral 84:1843–1849
Spiekermann G, Steel-McInnis M, Schmidt C, Jahn S (2012) Vibrational mode frequencies of silica species in SiO_2-H_2O liquids and glasses from ab initio molecular dynamics. J Chem Phys 136:154501
Stolen RH, Walrafen GE (1976) Water and its relation to broken bond defects in fused silica. J Chem Phys 64:2623–2631
Stolper A (1982) Water in silicate glasses: an infrared spectroscopic study. Contribut Mineral Petrol 81:1–17
Tarantola, A. (2005) Inverse problem theory and methods for model parameter estimation. Society of Industrial and Applied Mathematics
Thomas N, Jaupart C, Vergniolle S (1994) On the vesicularity of pumice. J Geophys Res 99:15633–15644
Tischendorf B, Ma C, Hammersten E, Venhuizen P, Peters M, Affatigato M, Feller S (1998) The density of alkali silicate glasses over wide compositional ranges. J Non Cryst Solids 239:197–202
Virgo D, Mysen BO, Kushiro I (1980) Anionic constitution of silicate melts quenched at 1 atm from Raman spectroscopy: implications for the structure of igneous melts. Science 208:1371–1373
Voigt U, Lammert H, Eckert H, Heuer A (2005) Cation clustering in lithium silicate glasses: quantitative description by solid-state NMR and molecular dynamics simulations. Phy Rev B 72:064207–1–11
Whittaker EJW, Muntus R (1970) Ionic radii for use in geochemistry. Geochim Cosmochim Acta 34:945–956
Wickersheim KA (1959) Infrared absorption spectra of lithium hydroxide. J Chem Phys 31:863–869
Wu C-K (1980) Nature of incorporated water in hydrated silicate glasses. J Am Ceram Soc 63:453–457
Xue X (2009) Water speciation in hydrous silicate and aluminosilicate glasses: direct evidence from ^{29}Si-^{1}H and ^{27}Al-^{1}H double-resonance NMR. Am Mineral 94:395–398
Xue X, Kanzaki M (2004) Dissolution mechanisms of water in depolymerized silicate melts: constraints from ^{1}H and ^{29}Si NMR spectroscopy and *ab initio* calculations. Geochim Cosmochim Acta 68:5027–5057
Xue X, Kanzaki M (2006) Depolymerization effect of water in aluminosilicate glasses: direct evidence from ^{1}H-^{27}Al heteronuclear correlation NMR. Am Mineral 91:1922–1926
Xue X, Kanzaki M (2008) Structure of hydrous aluminosilicate glasses along the diopside—anorthite join: a comprehensive one- and two-dimensional ^{1}H and ^{27}Al NMR study. Geochim Cosmochim Acta 72:2331–2348
Xue X, Kanzaki M (2009) Proton distributions and hydrogen bonding in crystalline and glassy hydrous silicates and related inorganic materials: insights from high-resolution solid-state nuclear magnetic resonance spectroscopy. J Am Ceram Soc 92:2803–2830
Yamashita S, Behrens H, Schmidt BC, Dupree R (2008) Water speciation in sodium silicate glasses based on NIR and NMR spectroscopy. Chem Geol 256:231–241
Zotov N, Keppler H (1998) The influence of water on the structure of hydrous sodium tetrasilicate glasses. Am Mineral 83:823–834

Submit your manuscript to a SpringerOpen journal and benefit from:

► Convenient online submission
► Rigorous peer review
► Immediate publication on acceptance
► Open access: articles freely available online
► High visibility within the field
► Retaining the copyright to your article

Submit your next manuscript at ► springeropen.com